IEEE Photonics Journal
An IEEE Photonics Society Publication

Improved Sensitivity RF Photonics Doppler Frequency Measurement System

Volume 8, Number 5, October 2016

Hossein Emami, ***Member, IEEE***
Mohammadreza Hajihashemi
Sayed Ehsan Alavi

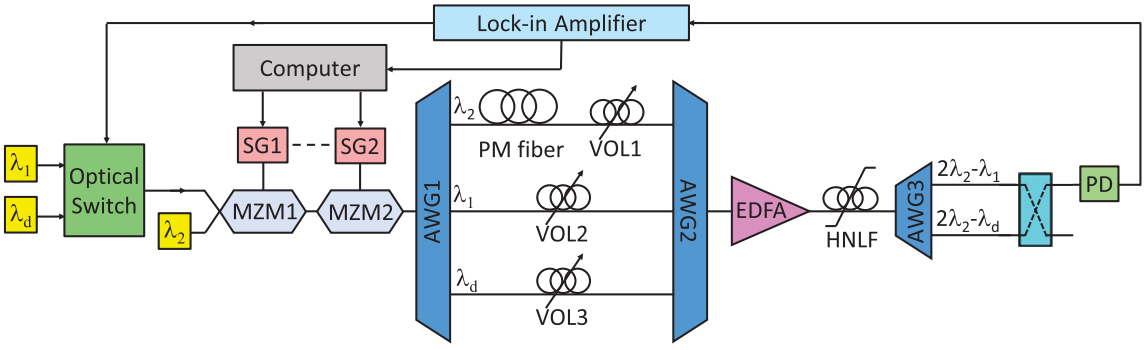

DOI: 10.1109/JPHOT.2016.2598787
1943-0655 © 2016 IEEE

Improved Sensitivity RF Photonics Doppler Frequency Measurement System

Hossein Emami,[1] ***Member, IEEE*****, Mohammadreza Hajihashemi,**[2] **and Sayed Ehsan Alavi**[3]

[1]Center for Advanced Engineering Research, Majlesi Branch, Islamic Azad University, Isfahan 8631656451, Iran.
[2]Department of Biomedical Engineering, University of Florida, Gainesville, FL 32611 USA.
[3]Faculty of Electrical Engineering, Universiti Teknologi Malaysia, 81310 Johor Bahru, Malaysia.

DOI:10.1109/JPHOT.2016.2598787

Manuscript received July 8, 2016; revised July 31, 2016; accepted August 5, 2016. Date of publication August 10, 2016; date of current version September 2, 2016. This work was supported by the Research University grant of Universiti Teknologi Malaysia under the Vot nos. 1) 09H77 and 2) 13H87.
Corresponding author: H. Emami (e-mail: h.emami@iaumajlesi.ac.ir).

Abstract: An improved sensitivity Doppler frequency measurement system based on microwave photonics technology was demonstrated practically. The system employs a four-wave mixing effect to achieve broad radio-frequency (RF) frequency measurement. In addition, a lock-in amplification technique was utilized to achieve high-measurement sensitivity. The system is, thus, capable of Doppler frequency estimation of radar echoes with a carrier frequency up to 40 GHz and a power level as low as −35 dBm.

Index Terms: Microwave photonics, microwave photonics signal processing.

1. Introduction

Doppler shift caused by target movement is one of the most important parameters in a radar system [1]. Fast and accurate measurement of the Doppler frequency have been always on demand and many electrical approaches have been proposed regarding Doppler frequency estimation (DFE) [2], [3]. Modern electronic warfare (EW) systems are moving to broadband operation in order to provide data security, effective target detection and better counter measure performance. As a result, radar systems operating based on frequency agility technique have been developed in recent years. These radars are specifically immune to enemy's jamming operation. As jamming techniques are becoming more advanced, the need to enhance the frequency agile radars is also felt. One parameter to be considered is the range within which the frequency agility is performed. The wider this range is, the harder the jamming system will interfere the radar operation. The radar systems that benefit from broad frequency agility range do need DFE. Current DFE systems are implemented in intermediate frequency (IF) or baseband section of the radar receiver. However, down-conversion itself in case of broad frequency agility is a bottleneck due to frequency dependent conversion gain of current down-converters [4], [5].

The echo received by a radar antenna is usually a weak signal. This would make the DFE even harder. In practice, low noise amplifiers (LNAs) are employed to amplify the echo signal to reach a level at which effective DFE becomes possible. The LNAs have limited bandwidth in order to effectively suppress the white noise received by the radar antenna and consequently achieve a

better noise figure. On the other hand, in a frequency agile system, broad frequency operation is required for all parts in the system including LNA. Implementation of such LNA could be hard as broadband operation opposes the low noise figure. Hence, it would be advantageous to implement a DFE system capable of operation with weak radar echoes with no radio-frequency (RF) amplification and with arbitrary radar carrier frequency.

Microwave photonics (MWP) technology has been introduced as a means of frequency independent signal processing [6]–[12]. Several attempts have thus been done on DFE schemes based on MWP. In an attempt, a two-path system consisting of a Doppler information to optical sideband converter and an optical frequency shifter was conceived and practically demonstrated [13]. An electrical spectrum analyzer was employed in order to analyze the system output and to extract the Doppler frequency. The system was able to perform DFE on radar carriers with a maximum frequency of 20 GHz.

In another work, both the transmitted radar signal and the received radar echo were mapped to two optical sidebands [14]. The two sidebands were beat together and the low-frequency Doppler shift was measured using an electrical spectrum analyzer. The system performance was demonstrated at 10, 15 and 30 GHz frequencies. Theoretical results showed that the system is able to operate with a minimum SNR of -19 dB at a 10 GHz carrier frequency.

An MWP I/Q detector was demonstrated in [15]. The system employed Hilbert transform to achieve in-phase and quadrature-phase signals. The system was also capable of becoming electrically reconfigured in order to detect Doppler shifts on any radar signal with up to 35 GHz carrier frequency. The Doppler frequency was identified using a digital oscilloscope.

We have developed a class of DFE systems capable of performing Doppler shift measurement with arbitrary radar carrier frequency up to 40 GHz [16]. The system operation is standalone which means no sophisticated and thus expensive electronic equipment is required to perform the measurement. However, the sensitivity of the system has remained in question.

In this paper, we first characterize the system of [16] in terms of sensitivity. Then, using lock-in amplification technique, the sensitivity of the system is improved by more than 31 dB.

The paper is organized as follows. Section 2 discusses the original DFE system and provide information regarding the system sensitivity characterization. In Section 3, we introduce lock-in amplification technique to enhance the system sensitivity. Discussions on the system performance and also suggestions for future works are provided in Section 4. Section 5 concludes the paper.

2. Original DFE System

In this section, we present the original DFE system of [16] and characterize the system sensitivity.

2.1 System Setup

Fig. 1 shows the experimental setup of the original DFE system. A laser array provided two optical carriers (λ_1 and λ_2). These carriers entered a Mach-Zehnder modulator (MZM1, Thorlabs, LN05S-FC, 3 dB bandwidth: 35 GHz). MZM1 was fed with an RF single tone with angular frequency of Ω_c produced by a signal generator (SG1, Anritsu, MG3690B). The MZM1 output became the MZM2 input. MZM2 was fed with another RF tone from SG2 with angular frequency $\Omega_c + \Omega_d$. Both MZMs were biased at positive quadrature point. The result was input to an array waveguide grating (AWG1, JDSU, FFC-MUX-017D) within which each optical carrier was separated. λ_1 was then delayed with respect to λ_2 using a length of polarization maintaining (PM) fiber and a PM variable optical length (VOL). Two signals were again combined within AWG2. The result was first amplified by a PM erbium-doped fiber amplifier (EDFA, PriTel PMFA-20) and entered a highly nonlinear fiber (HNLF, 1 km of OFS standard HNLF-zero dispersion at 1540 nm, dispersion slope: 0.019 ps/(nm.km), gamma: 21 /W/km) where many third order components were produced by Four-wave mixing from which the harmonic $2\lambda_2 - \lambda_1$ was separated by AWG3. The result was then input to a photo-detector (PD). The PD output was low-pass filtered (LPF) and was measured by a digital voltmeter (Agilent

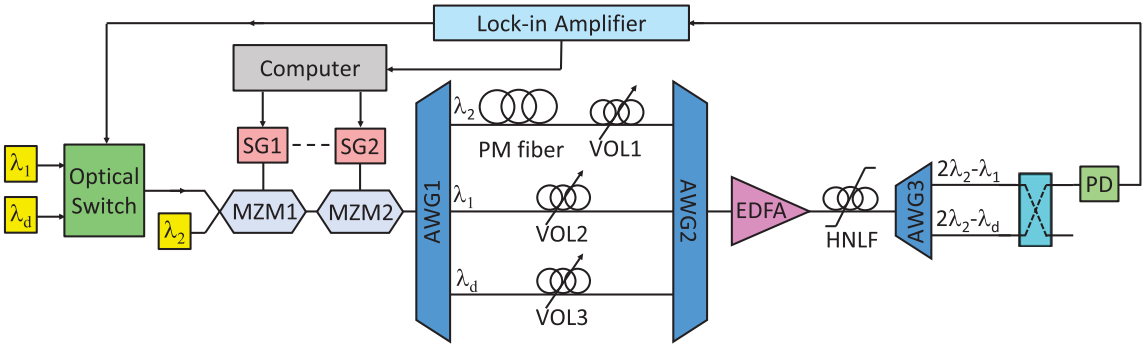

Fig. 1. Experimental setup of the original MWP DFE system.

3458A multimeter). A desktop computer gathered the voltmeter data and controlled SG1 and SG2. The SG1 reference output was connected to the SG2 reference input.

2.2 System Model

It can be shown that the output of the system of Fig. 1 is governed by [16]

$$V = A\left(1 - 8\alpha_1^2\alpha_2^2\cos 2\Omega_c\tau - 8\alpha_1^2\alpha_2^2\cos\Omega_d\tau\right) \tag{1}$$

where $A = \frac{9}{64}\Re G_{LPF} L_{AWG} G_c P_{in}^3 Z_L$, and $\Re$ denotes the PD responsivity. G_{LPF} and L_{AWG} are the LPF gain and each AWG optical insertion loss, respectively. Here, the same insertion loss is assumed for all AWGs. Z_L denotes the load impedance on PD. τ is the delay between λ_1 and λ_2 caused by PM fiber and VOL. P_{in} is the optical power of each wavelength at the input of HNLF and is given by $P_{in} = P_\circ L^2 L_{AWG}^2 G$ where $P_\circ$ denotes the optical power of each optical carrier. L and G are each MZM optical insertion loss and EDFA gain, respectively. α_1 and α_2 denote the modulation indices of MZM1 and MZM2, respectively, and are given by

$$\alpha_i = \frac{\sqrt{2}\pi(M P_{RF_i} Z_{in})^{\frac{1}{2}}}{2V_\pi} \quad i = 1, 2 \tag{2}$$

where M and P_{RF_i} are each MZM RF response and RF input power to each MZM, respectively. Z_{in} is each MZM RF input impedance. V_π denotes each MZM half-wave voltage. Here, it is assumed that both MZMs are identical.

2.3 System Characterization

The system of Fig. 1 was configured. It was aimed to cover a range of 0-456 kHz corresponding to a target speed range of 0 to Mach 10 at 40 GHz, and therefore, a value of 1 μs for the delay τ was set as described in [16]. The wavelengths λ_1 and λ_2 were set to 1534.97, and 1536.69 nm, respectively. Each laser power was adjusted such that it launches a 10 dBm power at the HNLF input. SG1 output signal was set to 0 dBm at 10 GHz. SG2 output signal was initially set to 10 dBm at 10 GHz. Then, SG2 swept a range of 10 to 10.456 GHz by incremental steps of 100 Hz. At each step, the digital voltmeter measured the voltage and sent data to the computer. The procedure was repeated at 20, 30, and 40 GHz frequencies, as well.

Fig. 2(a) shows the measured voltage versus the Doppler frequency for four different radar carrier frequencies (10, 20, 30, and 40 GHz) at 0 dBm echo power. As the Doppler frequency increases, the voltage increases as predicted by (1). A cosine shape for all curves can also be seen. For higher radar carriers the amplitude of the cosine curve is lower and the curve is noisier. Both can be attributed to the lower modulation indices (α_1 and α_2) at higher radar carriers. Remind that the modulation index is directly proportional to square root of RF frequency response of MZMs (M)

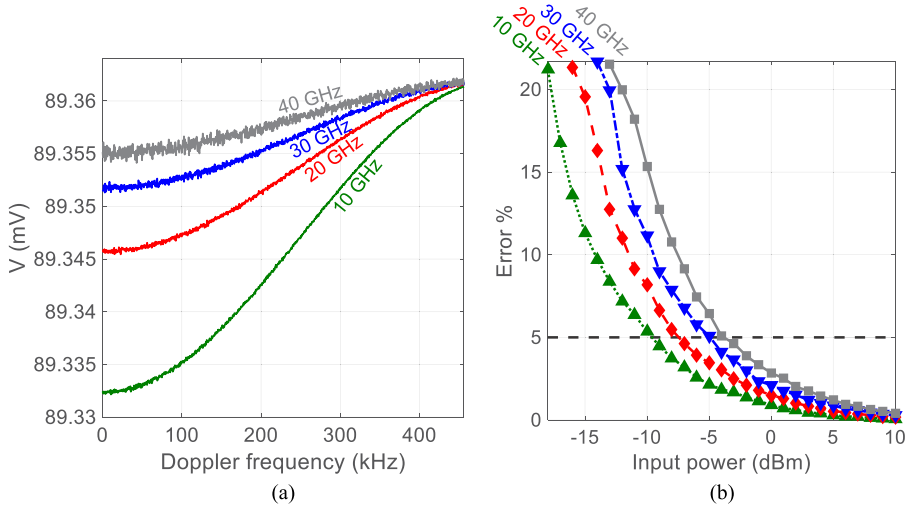

Fig. 2. (a) Output voltage vs. Doppler frequency at different radar carrier frequencies with echo power of 0 dBm. (b) Maximum frequency measurement error percentage.

as (2) indicates. Importantly, a huge offset of approximately 89 mV accompanies each cosine curve, which is also expected from (1).

In a radar receiver, sensitivity plays an important role. Therefore, to further investigate the possibility of utilizing the system of Fig. 1 in real applications, it is necessary to quantify the system sensitivity. To do this, the above procedure was repeated for various echo power levels starting from 10 dBm. Using (1), the Doppler frequency was calculated and the maximum measurement error was extracted. Then, the echo power level was decreased at 1 dB steps, and the error was calculated again. This procedure was continued until a maximum Doppler frequency measurement relative error of 20% was reached.

Fig. 2(b) shows maximum frequency measurement error percentage versus echo power for different carrier frequencies. As the input power decreases, the error increases as expected. Also, it can be seen that the error is larger at higher frequencies. For instance, to achieve a less than 5% error at 40 GHz, the RF power must not be less than -4 dBm while at 10 GHz, the RF input could be as low as approximately -10 dBm. This value for 20 and 30 GHz carrier frequencies is -7 and -5 dBm, respectively.

In real applications, the echo signal received by the radar antenna is much weaker. This makes the system of Fig. 1 inoperative. The sensitivity of the system must thus be improved.

3. Sensitivity Improvement

In this section, we present a scheme by which the sensitivity of the system of Section 2 would be increased.

3.1 Theoretical Background

We have established in Section 2.3 that the system of Fig. 1 has relatively poor sensitivity and thus is incapable of DFE at low RF powers. It is hypothesized that the relatively poor sensitivity of the system is due to the offset on the voltage curve as seen in Fig. 2(a). This offset makes the voltage measurement inaccurate. To further, explain this issue, we focus on (1). It can be seen that the voltage V has three terms. The first term is A which is a constant term. The second term is $-8A\alpha_1^2\alpha_2^2\cos 2\Omega_c\tau$. This term is a function of the radar carrier frequency Ω_c. However, this term is also constant when operating at a specific carrier frequency. The last term is $-8A\alpha_1^2\alpha_2^2\cos\Omega_d\tau$ which is the variable term and is a function of the Doppler frequency Ω_d. This term is in fact the

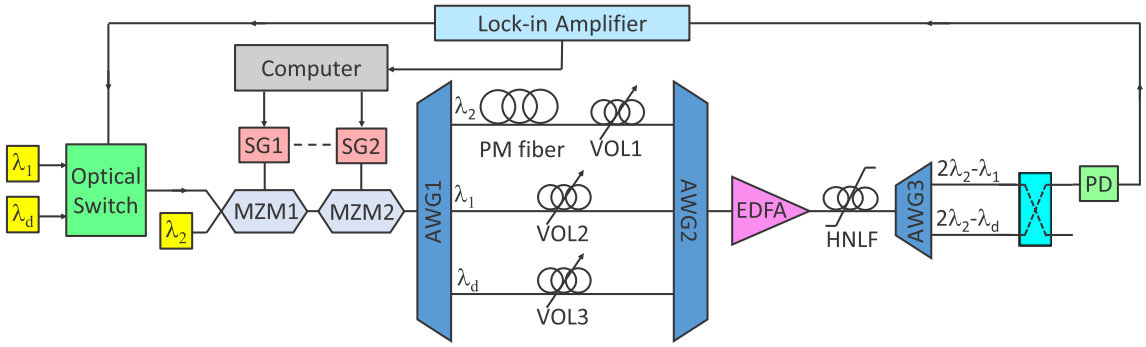

Fig. 3. Experimental setup of the improved sensitivity MWP DFE system.

desired term for DFE since it contains the actual data from which the Doppler frequency can be extracted. The absolute ratio of the DC offset (constant terms) to the amplitude of the third term (desired term) would be

$$r = \frac{|1 - 8\alpha_1^2\alpha_2^2 \cos 2\Omega_c\tau|}{|-8\alpha_1^2\alpha_2^2|}. \tag{3}$$

Note that the modulation indices have very small values. For instance, for an echo power of 10 dBm, the modulation index can be calculated using (2) as 0.31 assuming no RF dissipation for the MZM and a V_π of 5 V. Therefore, (3) can be simplified to

$$r = \frac{1}{8\alpha_1^2\alpha_2^2}. \tag{4}$$

This ratio is very large due to small modulation indices α_1 and α_2. For a modulation index of 0.31, r would be calculated to be approximately 13. Note that a modulation index of 0.31 is associated with 10 dBm RF power which is very high for an echo signal. Assuming a more realistic value of -10 dBm and a typical MZM RF loss of 3 dB, the ratio r would be calculated as approximately 5×10^5. It can thus be inferred that the measured voltage by the digital voltmeter remains almost constant when operating at low RF power levels and this obviously results in inaccurate voltage measurement and consequently an erroneous DFE. It is thus hypothesized that removing the DC offset from (1) would result in a better measurement accuracy. One solution could be lock-in amplification in which the desired term to be measured would be modulated by a single tone at a specific frequency while the unwanted terms would remain unmodulated [17]. On detection, the signal would be mixed again with the same tone. Here, the constant term will be omitted and only the desired term will remain. From (1), it can be seen that the only term that distinguished the third term form the other terms is the Doppler frequency Ω_d itself, which obviously cannot be modulated by the lock-in amplifier. However, another approach is to modulated the delay τ which is a common term between the second and the third term of (1) but does not exist in the first term.

Remind that the second term in (1) is much smaller than the first term since the second term contains small modulation indices as discussed in this section before. Therefore, it would be a reasonable solution to only eliminate the first term of (1) and to measure both the second and the third term together.

3.2 System Setup

We have hypothesized that the huge offset on the output voltage of the system of Fig. 1 is responsible for the huge measurement error and by removing this DC offset a better accuracy should be achieved. To prove this, the lock-in amplification technique must be employed in the system of Fig. 1 and the measurement results must be analyzed.

Fig. 3 shows the proposed experimental setup of the improved sensitivity DFE system. Compared with the system of Fig. 1, another optical carrier (λ_d) was used. An optical switch (Agiltron,

NSSW-125114323) was also employed to switch between λ_1 and λ_d continuously. The switch was controlled by the dithering signal of the lock-in amplifier (EG&G Princeton Applied Research Model 5210). Since there were three optical carriers, another port of AWG1 and AWG2 was used to separate λ_d. Also, another port of AWG3 was used to extract the harmonic $2\lambda_2 - \lambda_d$. Both ports of AWG3 was connected to an optical coupler. The output of the coupler was connected to PD. The rest of the system remained unchanged. It should be noted that at each time only one harmonic is present at AWG3 output ports since the optical switch allows only one carrier through at any time.

Having conceived a setup that utilizes lock-in amplification to enhance the DFE, the system must now be characterized.

3.3 System Characterization

The system was configured as shown in Fig. 3. λ_d was selected to be 1538.32 nm. All laser powers were set to exhibit 10 dBm power at the HNLF input. The rest of settings were the same as described in Section 2.3.

3.3.1 Delay Adjustment: The delay τ has a value of 1 μs. This delay must be modulated by the lock-in amplifier. The modulation procedure in lock-in amplification usually is done by dithering the selected variable (the delay τ in this experiment) by a small amount. We chose a dithering value of 2%. To dither the delay by this value, VOl1 and VOL2 were carefully adjusted such that one exhibits a 2% deviation from the delay with respect to the other one. The same procedure as described in Section 2.3 was performed to achieve 2% deviation for 1 μs. This time, VOLs1-3 were adjusted such that λ_1 and λ_d had delays of 0.99τ and 1.01τ with respect to λ_2, respectively.

3.3.2 Lock-In Amplifier Parameters: The lock-in amplifier settings were as follows. The oscillator was set to generate a square-wave at 1 kHz. The dithering signal was chosen to be square-wave to enable effective operation of the optical switch. The oscillator frequency was set to 1 kHz to enable use of in-expensive low-frequency photo-detectors in the system. Lower frequencies would decrease the system response which may not be of interest for frequency agile systems. The input filter was set to be band-pass in order to reject all DC residuals (unwanted terms in (1). This would also remove the need to operate at high dynamic reserve mode. The ratio of the unwanted terms to the desired term in (1) was calculated to be 5×10^5 in Section 3.1. This would need at least a dynamic reserve of 114 dB. The lock-in amplifier is capable of providing such dynamic reserve; however, this would be at the cost of sacrificing the measurement stability. On the other hand, by setting the input filter operation to band-pass no DC component could pass through to saturate the amplifier. Therefore, a lower dynamic reserve and consequently higher stability operation becomes possible. Hence, the amplifier was configured to operate at high stability mode with 90 dB dynamic reserve providing 5 ppm/$^\circ$C stability. As Fig. 2(a) shows, the input of the lock-in amplifier is approximately 89 mV. Thus, 100 mV full-scale was chosen. At this amount, the amplifier could provide 10 dB gain. The output LPF slope was set to 12 dB/Oct to achieve better noise rejection. The LPF time constant was set to 1 ms. Note that the dominant delay in the entire system is determined by this time constant. Thus, the system latency is approximately 1 ms. Although a higher time constant will result in better stability; however, it will also result in higher latency which may not be desirable in an EW system.

3.3.3 Results: Fig. 4(a) shows the recorded voltage by the lock-in amplifier versus the Doppler frequency at different radar carrier frequencies with 0 dBm echo power level. The previous results from Fig. 2(a) are also provided to enable easy comparison. The voltage offset is decreased drastically by the lock-in amplifier as expected. Note that the first term in (1) is mainly responsible for the DC offset which has been removed by the lock-in amplifier. The second term (small DC offset) and the third term (desired term) have still remained. The system sensitivity should now be improved. To investigate this, the procedure of error measurement was repeated as described in Section 2.3 and the results are shown in Fig. 4(b). The measurements from the system of Fig. 1 are also provided for comparison purposes. Better sensitivity is indeed achieved as expected. At 10 GHz carrier frequency an error of 5% occurred at -41 dBm which shows more than 31 dB improvement compared to the response of Fig. 1. At the worst-case scenario (40 GHz carrier

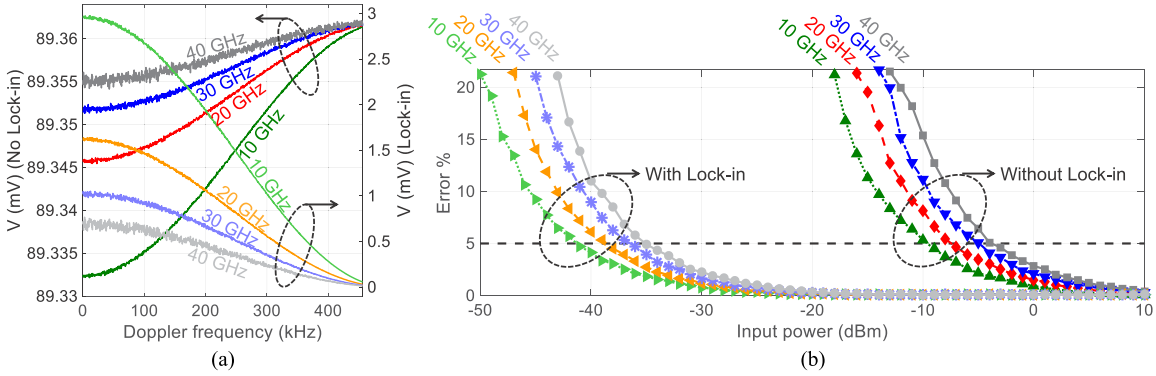

Fig. 4. (a) Measured voltage vs. Doppler frequency at different radar carrier frequencies with echo power of 0 dBm with and without lock-in amplification. (b) Maximum frequency measurement error percentage with and without lock-in amplification.

frequency), the 5% error happened at −35 dBm. Again 31 dB improvement can be seen in this case. This is also true for 20 and 30 GHz carrier frequencies. Hence, it can be confirmed that the lock-in amplification has indeed improve the system sensitivity.

4. Discussion and Suggestions for Future Work

It has been demonstrated that using lock-in amplification would result in at least 31 dB improvement in the system sensitivity. This is very crucial in an EW environment where echo signals are usually weak. This sensitivity was achieved without the use of any wideband high-frequency pre-amplification, which would also result in better system stability since usually wideband high gain amplifiers tend to oscillate and stabilization is always a problem.

MZM bias controllers are obviously required for long term operation. Fortunately, very advanced yet inexpensive bias controllers have already been developed and are commercially available [18]. Another channel of the lock-in amplifier itself could also be used for such purpose.

The main bottleneck of the system that prevents the system to operate at frequencies beyond 40 GHz is the MZMs cut-off frequency. Lithium Niobate electro-optic modulators with operation frequency up to 300 GHz [19] could be employed for such purpose. Note that since the system employs Four-wave mixing as a mixing tool, the rest of the system is broadband for decades of gigahertz. This way, the system could be employed in W-band radars operating at 210 GHz frequency [20].

The system has potential to be integrated. In this case, the HNLF could be replaced by an ultra-compact long silicon strip waveguide [21]. Photonic crystal waveguide could also be considered for such purpose [22]. This way, it would be possible to achieve both nonlinear optical mixing and optical delay on-chip which would further simplify the system and will result in further cost and size reduction. This would also remove the need for an EDFA since the efficiency of such waveguide is higher than that of HNLF.

5. Conclusion

We have practically demonstrated a scheme by which the Doppler shift on weak radar echoes can be detected. The system exhibits only 5% error when measuring the Doppler frequency on a radar echo as weak as −35 dBm at 40 GHz carrier. The same error was obtained at −41 dBm when the radar carrier was 10 GHz. No electrical amplification was required for the echo signal to be detected. This sensitivity was achieved using lock-in amplification technique. Suggestions for performance improvement were also provided.

References

[1] M. I. Skolnik, *Introduction to Radar Systems*, 3rd ed. New York, NY, USA: McGraw-Hill, 2001, ch. 13.
[2] L. Han and K. Wu, "24-GHz integrated radio and radar system capable of time-agile wireless communication and sensing," *IEEE Trans. Microw. Theory Techn.*, vol. 60, no. 3, pp. 619–631, Mar. 2012.
[3] J. F. Gu, J. Moghaddasi, and K. Wu, "Delay and doppler shift estimation for OFDM-based radar-radio (RadCom) system," in *Proc. IEEE Int. Wireless Symp.*, Shenzhen, 2015, pp. 1–4.
[4] C. C. Su, C. H. Liu, C. M. Lin, Y. L. Tsai, and Y. H. Wang, "A 24-44 GHz broadband subharmonic mixer with novel isolation-enhanced circuit," *IEEE Microw. Wireless Compon. Lett.*, vol. 25, no. 2, pp. 124–126, Feb. 2015.
[5] S. J. Mahon *et al.*, "Broadband integrated millimeter-wave up- and down-converter GaAs MMICs," *IEEE Trans. Microw. Theory Techn.*, vol. 54, no. 5, pp. 2050–2060, May 2006.
[6] J. Capmany and D. Novak, "Microwave photonics combines two worlds," *Nature Photon.*, vol. 1, no. 6, pp. 319–330, Jun. 2007.
[7] W. Zhang and R. A. Minasian, "Switchable and tunable microwave photonic Brillouin-based filter," *IEEE Photon. J.*, vol. 4, no. 5, pp. 1443–1455, Oct. 2012.
[8] W. Li and J. Yao, "Microwave and terahertz generation based on photonically assisted microwave frequency twelvetupling with large tunability," *IEEE Photon. J.*, vol. 2, no. 6, pp. 954–959, Dec. 2010.
[9] N. Sarkhosh, H. Emami, L. Bui, and A. Mitchell, "Photonic instantaneous frequency measurement using non-linear optical mixing," in *Proc. IEEE MTT-S Int. Microw. Symp. Dig.*, Atlanta, GA, USA, 2008, pp. 599–601.
[10] P. Ghelfi *et al.*, "A fully photonics-based coherent radar system," *Nature*, vol. 507, pp. 341–345, Mar. 2014.
[11] M. Zhang, Y. Ji, Y. Zhang, Y. Wu, H. Xu, and W. Xu, "Remote radar based on chaos generation and radio over fiber," *IEEE Photon. J.*, vol. 6, no. 5, pp. 1–12, Oct. 2014.
[12] C. H. Cheng, Y. C. Chen, and F. Y. Lin, "Generation of uncorrelated multichannel chaos by electrical heterodyning for multiple-inputmultiple-output chaos radar application," *IEEE Photon. J.*, vol. 8, no. 1, pp. 1–14, Feb. 2016.
[13] B. Lu, W. Pan, X. Zou, X. Yan, L. Yan, and B. Luo, "Wideband Doppler frequency shift measurement and direction ambiguity resolution using optical frequency shift and optical heterodyning," *Opt. Lett.*, vol. 40, no. 10, pp. 2321–2324, May. 2015.
[14] X. Zou, W. Li, B. Lu, W. Pan, L. Yan, and L. Shao, "Photonic approach to wide-frequency-range high-resolution microwave/millimeter-wave Doppler frequency shift estimation," *IEEE Trans. Microw. Theory Techn.*, vol. 63, no. 4, pp. 1421–1430, Apr. 2015.
[15] H. Emami and N. Sarkhosh, "Reconfigurable microwave photonic in-phase and quadrature detector for frequency agile radar," *J. Opt. Soc. Amer. A*, vol. 31, no. 6, pp. 1320–1325, Jun. 2014.
[16] H. Emami, M. Hajihashemi, and S. E. Alavi, "Standalone microwave photonics Doppler shift estimation system," *J. Lightw. Technol.*, vol. 34, no. 15, pp. 3596–3602, Aug. 2016.
[17] A. Schneider, "Enhancing the amplitude of terahertz transients using lock-in amplification and a spinning nonlinear crystal," *IEEE Trans. THz Sci. Technol.*, vol. 4, no. 5, pp. 605–608, Sep. 2014.
[18] ID Photonics GmbH, "Automatic Mach Zehnder BIAS control (Extended Datasheet)," [Online]. Available: www.xsoptix.com/data/idphotonics/ds_idp_ABC-x-x-xx_extended.pdf
[19] J. Macario *et al.*, "Full spectrum millimeter-wave modulation," *Opt. Exp.*, vol. 20, no. 21, pp. 23623–23629, Oct. 2012.
[20] A. Tessmann *et al.*, "Metamorphic HEMT MMICs and modules for use in a high-bandwidth 210 GHz radar," *IEEE J. Solid-State Circuits*, vol. 43, no. 10, pp. 2194–2205, Oct. 2008.
[21] M. Pagani *et al.*, "Low-error and broadband microwave frequency measurement in a silicon chip," *Optica*, vol. 2, no. 8, pp. 751–756, Aug. 2015.
[22] M. Ebnali-Heidari, C. Monat, C. Grillet, and M. K. Moravvej-Farshi, "A proposal for enhancing four-wave mixing in slow light engineered photonic crystal waveguides and its application to optical regeneration," *Opt. Exp.*, vol. 17, no. 20, pp. 18340–18353, Sep. 2009.